Regular Article

Tuning of nonlinear optical characteristics of Mathieu quantum dot by laser and electric field

M. K. Bahar[a], **P. Başer**[b]

Department of Physics, Faculty of Science, Sivas Cumhuriyet University, 58140 Sivas, Turkey

Abstract In this work, for the first time, the total refractive index (TRICs) and total absorption coefficients (TACs) of $In_xGa_{1-x}As/GaAs$ Mathieu quantum dot (MQD) with hydrogenic impurity under the influence of the external electric field and laser field are probed. Within the framework of the Ehlotzky approximation, considering the Kramers–Henneberger transformation and dipole approximation, the time-dependent in the wave equation is transferred from the kinetic energy operator to the potential energy function. Then, the new Schrödinger equation for the MQD including the hydrogenic impurity under the external electric field and monochromatic linearly polarized laser radiation is solved numerically by employing the tridiagonal matrix method. In order to study the TRICs and TACs of MQD, the iterative method and compact-density-matrix formalism are employed. The influence of structural parameters as well as the external factors on the TRICs and TACs of the MQD is examined. The effects of external electric field, laser field, *In*-concentration, impurity atom position, the MQD depth and width parameters on the TRICs and TACs are investigated in detail, and functional ranges of relevant parameters are also determined for the purpose. In addition, the alternatives of these parameters to each other are also discussed. It is important for experimental research that all parameter values used are accessible.

1 Introduction

Semiconductor quantum dots are nanometer-sized materials composed of 10^2–10^5 atoms. This size is small enough to restrict particle movement in three dimensions. Quantum dots may also be taken into considered as artificial atoms. Semiconductor quantum dots can be produced in high quality thanks to the advancement of epitaxial growth techniques of heterostructures [1]. Zero-dimensional quantum dots become very attractive for optical applications and new technologies due to their high efficiency, tunable electronic properties through alloy concentration, and long lifetimes. In spherical quantum dots, the critical radius value depends on strongly the band offset value, which is related to the energy bandgap of the material system used. Some optical applications of quantum dots can be listed as light emitting diodes, solid state illuminated displays, photovoltaics and infrared photodetectors [2–5]. Also, since quantum dots have a sharper state density compared to quantum wires and quantum wells, devices that contain these structures and therefore work faster and more efficiently can be designed. Among these applications, transistors, solar cells, optical switches and logic gates are the most important ones [6–9].

Different interaction potential energies affect the optical and electronic properties of quantum dots, as expected. In this manner, the quantum dot consisting of $In_xGa_{1-x}As/GaAs$ heterostructure with Mathieu potential encompassment has been considered, and some nonlinear optical properties have been investigated under the external electric and magnetic field [10]. Mathieu functions have been employed in the one-dimensional periodic Schrödinger equation formalism including a potential energy function consisting of a symmetric or asymmetric barrier and a well [11]. As well-known, except for harmonic oscillator and hydrogen atom potentials, the exact analytical solution of the nonrelativistic and relativistic wave equations for many potentials is quite difficult. However, the eigenvalue equations of potentials in the class X, which are called semisolvable, could be solved [12]. In the present work, GaInAs is considered as the material for the MQD. The GaInAs ternary semiconductor compound is greatly attractive for optoelectronic designs due to its wide band gap that can be changed from 0.42 to 1.52eV using the *In* concentration [13]. $In_xGa_{1-x}As$ has high electron mobility, and some of its applications can be exemplified as solar cells [14], high electron mobility transistors [15], lasers [16], modulators [17] and detectors operating in the short wavelength infrared region [18]. Therefore, this material is very plausible for III-V-based quantum dots. As the external electric and laser field applied on low-dimensional structures have remarkable impressions on the symmetry of the structure and the effective confinement potential shielding, electronic energy levels and transition processes

[a] e-mail: mussiv58@gmail.com (corresponding author)

[b] e-mail: pbaser34@gmail.com

between levels. Therefore, the transitions between the subbands, which are directly related to the electronic and optical properties of the structure, can be controlled by external fields. Applied external fields are an effective argument to control and modulate electronic and optical properties of related structure [19]. For this reason, many studies have taken into account the functionalities of laser and electric field on the linear optical and electronic properties of the system [20–23]. In the most of theoretical studies, well-like potentials prefer as the confinement potential due to their convenience to fabricate experimentally. The Rosen-Morse potential is a reasonable one for experimental suitability. In this context, it has been investigated that how to affect the laser field the TRICs and TACs of the GaAs/GaAlAs Rosen-Morse quantum well, and it has been determined that the laser parameter is very effective on the TRICs and TACs amplitudes [20]. In addition, nonlinear optical rectification (NOR) and optical absorption coefficients (OACs) of GaAs/AlGaAs semiparabolic quantum wells under the effect of external electric and magnetic field have been investigated by using the finite difference method, in which results show that the NORs and OACs are highly dependent on the applied electric field strength [22]. As the applied electric field increases, the resonant peaks of the NOR decrease and shift to blue. These changes are very significant for device applications based on energy transitions [22]. As well as the efficiency of the laser and external electric field on the linear optical features, it has also been observed that they modifies nonlinear optical properties such as second harmonic generation (SHG), third harmonic generation (THG) and nonlinear optical rectification (NOR) [23–25]. In inverse V-shaped quantum wells modulated by high-frequency laser field, it has been observed that the amplitude values of the SHG coefficients increase because of augmenting laser field strength, and the relevant resonant frequencies shift to red [23]. Impurities have an indispensable role in semiconductor technology. Therefore, impurity cases in semiconductors have been widely studied theoretically and experimentally [26, 27]. In addition, the laser field applied to the impurity-containing structure changes considerably the electronic properties, because of the laser-triggered Coulomb potential caused by the laser radiation. A noticeable change in the magnitude of the binding energy has been obtained in the presence of an intense laser field [28]. The optical absorption and refractive index of the donor impurity confined by a three-dimensional quantum pseudodot have been investigated using the matrix diagonalization method [29], in which a greater optical nonlinearity is obtained by changing the zero point of the pseudoharmonic potential compared to the chemical potential of the electron gas. Both the second harmonic and third harmonic coefficients are greater, compared to the no impurity case, for an impurity atom placed in the repulsive region of the potential [30]. Because of the remarkable results of the impurity atom, the impurity effect is an important factor worth-examining. In the present work, the different placed-impurity atom effect, electric-laser field effect, as well as the quantum dot radius and potential parameters on the TRICs and TACs have been investigated in detail in a cause-effect relationship. The Mathieu encompassment that is considered as a quantum dot confinement potential, can also lead to experimental studies since it can be grown as a well-like structure with advanced crystal growth techniques. Another remarkable effect on the TRICs and TACs is noise. The noise effects create important findings in controlling and improving the performance of quantum dot devices. In this manner, the Gaussian white noise effects on the optical refractive index and total absorption coefficients of white noise driven, impurity doped parabolic GaAlAs-based quantum dot under external electric and magnetic field have been investigated [31–33]. In these studies, the external fields, impurity contribution and Gaussian white noise effects have been analyzed in consideration of the optical refractive index and absorption coefficients. The most important and common result of these studies in terms of Gaussian white noise is that Gaussian white noise is a functional influence on the optical refractive index and absorption coefficients, both in terms of resonant frequencies and optimality, within other physical conditions considered, and has the potential for significant technological findings.

The obtained results show that the TRICs and TACs depend on closely quantum dot sizes, impurity location and external fields. The influence of both structural and external parameters on the TRICs and TACs has been described in detail. In addition to determining the optimal ranges of structural and external parameters, their alternatives to each other have been also investigated, which in turn is significant in terms of determining of different experimental arguments with the same functions. Moreover, since a critical value of the impurity atom has been revealed, a detailed analysis has also been carried out on it. All investigations have been carried out within experimentally achievable parameter ranges, which is extremely important for applicability.

The article is organized as follows: Sect. 2 outlines the theoretical model and the relevant procedures. In Sect. 3, the results obtained are presented and interpreted in detail. Section 4 is allocated to summary and conclusions.

2 Theoretical model

The time-dependent Schrödinger equation for the MQD including the hydrogenic impurity under the external electric field and monochromatic linearly polarized laser radiation is given by

$$\left[\frac{(\mathbf{P} + \frac{e}{c}\mathbf{A}(\mathbf{r}, \mathbf{t}))^2}{2m^\star} + V_{\mathrm{MQD}}(r) + V_H(|r - r_i|) + e\xi\mathbf{r} \right] \Psi(\mathbf{r}, t) = i\hbar \frac{\partial \Psi(\mathbf{r}, t)}{\partial t}, \tag{1}$$

where $V_{\mathrm{MQD}}(r)$ is the MQD potential, $V_H(|r - r_i|)$ is the hydrogenic impurity potential with the impurity location r_i, ξ is the external electric field strength. The electromagnetic field in Eq.(1) relates to the vector potential $\mathbf{A}(\mathbf{r}, t)$ through $F = \frac{\partial A}{\partial t}$ (F contains the electric and magnetic field components of the electromagnetic radiation field [34]) in consideration of $\nabla.\mathbf{A} = 0$ and scalar potential $\Phi(\mathbf{r}) = 0$ in the Coulomb gauge. The time dependency in the Schrödinger equation can be modified by employing the

dipole approximation [35] and Kramers–Henneberger (KH) transformation [36, 37]. Being $\alpha(t)$ a vector for classical displacement, forming a center of oscillation along the polarization direction, it includes the oscillation frequency and the amplitude of the laser field. The effect of the external monochromatic linearly polarized laser radiation is attributed to $\alpha(t)$. The $\alpha(t)$ is calculated by employing time-dependent vector potential as follows:

$$\alpha(t) = \frac{e}{m} \int \mathbf{A}(t') \mathrm{d}t'. \tag{2}$$

For details, please refer [38]. Then, the time-dependent Schrödinger equation converts to the following form:

$$-\frac{\hbar^2}{2m^\star} \nabla^2 \chi(\mathbf{r}, t) + \left[V_{\mathrm{MQD}}[r + \alpha(t)] + V_H(|r - r_i| + \alpha(t)) + e\xi r \right] \chi(\mathbf{r}, t) = i\hbar \frac{\partial \chi(\mathbf{r}, t)}{\partial t}, \tag{3}$$

where $\chi(\mathbf{r}, t)$ is formed by the operator acting on the wave function. $\alpha(t)$ provides the transferring of time dependency in kinetic energy to potential energy. $\alpha(t) = \alpha_0 \sin(\omega t)$ with $\alpha_0 = \frac{eF_0}{m^\star \omega^2}$, where F_0 is the electromagnetic radiation field amplitude, ω is the angular frequency of the electromagnetic field. α_0 is called as the laser-dressing parameter which determines the laser field strength. The time dependency in the wave equation can be removed by considering the Fourier–Floquet series [39] and Ehlotzky approximation [40, 41]. Then, the relevant Schrödinger equation becomes the following form:

$$\left[-\frac{\hbar^2}{2m^\star} \nabla^2 + \frac{1}{2} \Big(V_{\mathrm{MQD}}(r + \alpha_0) + V_{\mathrm{MQD}}(r - \alpha_0) \Big) \right.$$
$$\left. + \frac{1}{2} \Big(V_H(|r - r_i| + \alpha_0) + V_H(|r - r_i| - \alpha_0) \Big) + e\xi r \right] P(r, \theta, \phi) = \mathrm{E}P(r, \theta, \phi) \tag{4}$$

For details in Eq. (4), please refer Refs. [42–44]. The MQD confinement potential is expressed as

$$V_{\mathrm{MQD}}(r) = V_0 \Big[\sin^2(\eta r) - \cos(\eta r) \Big], \tag{5}$$

where V_0 is the potential depth parameter, and there is its dependence to *In*-concentration as $V_0 = (1.42 - 1.53x + 0.45x^2)$ [45], η is the potential width parameter having 1/length dimension. The Coulomb potential for the hydrogenic impurity located in r_i from the origin is given by

$$V_H = -\frac{Ze^2}{4\pi\varepsilon_0\varepsilon|r - r_i|}, \tag{6}$$

where ε is the dielectric constant of the system while ε_0 is the vacuum dielectric constant. In Eq. (4), considering $P(r, \theta, \phi) = r^{-1} R(r) Y_\ell^m(\theta, \phi)$, the radial wave equation is obtained in the following form:

$$R''(r) + \left[\frac{2m^\star}{\hbar^2} (E - U_{eff}(r, \alpha_0, r_i, \ell)) \right] R(r) = 0, \tag{7}$$

where

$$U_{eff}(r, \alpha_0, r_i, \ell) = \frac{1}{2} \left[V_{\mathrm{MQD}}(r + \alpha_0) + V_{\mathrm{MQD}}(r - \alpha_0) \right] + \frac{1}{2} \left[V_H(|r - r_i| + \alpha_0) + V_H(|r - r_i| - \alpha_0) \right]$$
$$+ e\xi r + \frac{\ell(\ell + 1)\hbar^2}{2m^\star r^2}. \tag{8}$$

To solve Eq. (7), the tridiagonal matrix method (TMM) is used. For details, please refer [46].

The linear and nonlinear susceptibilities are procured through the density-matrix approach, they are expressed in closed analytical form as follows [47]

$$\varepsilon_0 \chi^{(1)}(\omega) = \frac{\sigma_v |M_{fi}|^2}{E_{21} - \hbar\omega - i\hbar\Gamma_{if}}, \tag{9}$$

$$\varepsilon_0 \chi^{(3)}(\omega) = -\frac{\sigma_v |M_{fi}|^2 |\tilde{E}|^2}{E_{fi} - \hbar\omega - i\hbar\Gamma_{if}}$$
$$\times \left[\frac{4|M_{fi}|^2}{(E_{fi} - \hbar\omega)^2 + (\hbar\Gamma_{if})^2} - \frac{(M_{ff} - M_{ii})^2}{(E_{fi} - i\hbar\Gamma_{if})(E_{fi} - \hbar\omega - i\hbar\Gamma_{if})} \right] \tag{10}$$

with σ_v (the carrier density), $E_{i,f}$ (the initial (i) and final (f) energy state), $\tilde{E}$ is the electromagnetic field amplitude, M_{fi} (being f, i the final and initial state, respectively, the dipole matrix elements ensured using $M_{fi} = \langle f|\mathbf{r}|i \rangle$), $\Gamma = 1/\tau$ is the relaxation rate for i, f states. Also, in computations of M_{if}, the following property of the spherical harmonics is taken into consideration [48],

$$\cos\theta Y_{\ell m}(\theta, \varphi) = Q_{\ell-1,m}Y_{\ell-1,m}(\theta, \varphi) + Q_{\ell,m}Y_{\ell+1,m}(\theta, \varphi), \tag{11}$$

where

$$Q_{\ell,m} = \left[\frac{(\ell+1)^2 - m^2}{(2\ell+1)(2\ell+3)} \right]^{1/2}. \tag{12}$$

Considering Eq. (11) and Eq. (12), it is found that [48]

$$\langle n'\ell'm' \mid r\cos\theta \mid n\ell m \rangle = (Q_{\ell-1,m}\delta_{\ell',\ell-1} + Q_{\ell,m}\delta_{\ell',\ell+1})I'_{n\ell n'\ell'}\delta_{m',m}, \tag{13}$$

where

$$I'_{n\ell n'\ell'} = \int_0^{R_{\text{dot}}} Q_{n\ell}Q_{n'\ell'}r\,\mathrm{d}r. \tag{14}$$

The dipole matrix elements are procured through Eq. (13) by regarding $\triangle\ell = \pm 1$. The linear and the third-order nonlinear RICs are expressed as [47]

$$\frac{\Delta n^{(1)}(\omega)}{n_r} = \frac{\sigma_v |M_{fi}|^2}{2n_r^2\varepsilon_0} \left[\frac{E_{fi} - \hbar\omega}{(E_{fi} - \hbar\omega)^2 + (\hbar\Gamma_{if})^2} \right], \tag{15}$$

$$\frac{\Delta n^{(3)}(\omega, I)}{n_r} = -\frac{\mu c |M_{fi}|^2}{4n_r^3\varepsilon_0} \frac{\sigma_v I}{[(E_{fi} - \hbar\omega)^2 + (\hbar\Gamma_{if})^2]^2}$$
$$\times [4(E_{fi} - \hbar\omega)|M_{fi}|^2 - \frac{(M_{ff} - M_{ii})^2}{(E_{fi})^2 + (\hbar\Gamma_{if})^2}\{(E_{fi} - \hbar\omega)$$
$$\times [(E_{fi})(E_{fi} - \hbar\omega) - (\hbar\Gamma_{if})^2] - (\hbar\Gamma_{if})^2(2(E_{fi}) - \hbar\omega)\}], \tag{16}$$

being μ, c the system permeability and the light speed in vacuum, respectively, I is the incident optical intensity. The TRIC is presented by adding the linear and nonlinear contributions [47]:

$$\frac{\Delta n(\omega, I)}{n_r} = \frac{\Delta n^{(1)}(\omega)}{n_r} + \frac{\Delta n^{(3)}(\omega, I)}{n_r}. \tag{17}$$

The linear and the third-order nonlinear ACs are expressed as

$$\alpha^{(1)}(\omega) = \omega\sqrt{\frac{\mu}{\varepsilon_r}} \frac{|M_{fi}|^2\sigma_v\hbar\Gamma_{if}}{(E_{fi} - \hbar\omega)^2 + (\hbar\Gamma_{if})^2}, \tag{18}$$

$$\alpha^{(3)}(\omega, I) = -2\omega\sqrt{\frac{\mu}{\varepsilon_R}}\left(\frac{I}{\varepsilon_0 n_r c}\right) \times \frac{|M_{fi}|^4\sigma_v\hbar\Gamma_{if}}{[(E_{fi} - \hbar\omega)^2 + (\hbar\Gamma_{if})^2]^2}$$
$$\left(1 - \frac{|M_{ff} - M_{ii}|^2}{|2M_{fi}|^2} \times \frac{(E_{fi} - \hbar\omega)^2 - (\hbar\Gamma_{if})^2 + 2(E_{fi})(E_{fi} - \hbar\omega)}{(E_{fi})^2 + (\hbar\Gamma_{if})^2}\right). \tag{19}$$

The TAC is represented by adding the linear and nonlinear contributions [47]:

$$\alpha(\omega, I) = \alpha^{(1)}(\omega) + \alpha^{(3)}(\omega, I). \tag{20}$$

For details, please refer [47].

It is important to note that the selection rules $\triangle\ell = \pm 1(m = 0)$ is taken into consideration in the present work. In addition, throughout the present work, some parameter values are considered as $m_{GaAs} = 0.067m_0$ (m_0 is mass of the free electron), $R_{dot} = 6a_0$, $\varepsilon_{GaAs} = 13.18$, $n_r = 3.2$ and $\tau = 0.2$ ps. In this case, the effective Rydberg energy and Bohr radius are computed as $R_y^* \cong 5.28$ meV and $a_0 = 103.7$ Å, respectively [49, 50].

3 Result and discussions

We investigate the effects of impurity location (r_i), *In* concentration (x), and quantum dot width (η) on the TRICs and TACs of spherical Mathieu quantum dot (MQD) under the influence of the external electric field and laser field. The first three electronic energy levels, the wave functions at their localizations and the relevant effective potential are represented, by taking into consideration the laser field strength (α_0) in Fig. 1a, the external electric field strength (ξ) in Fig. 1b, the impurity location (r_i) in Fig. 1c, *In* concentration
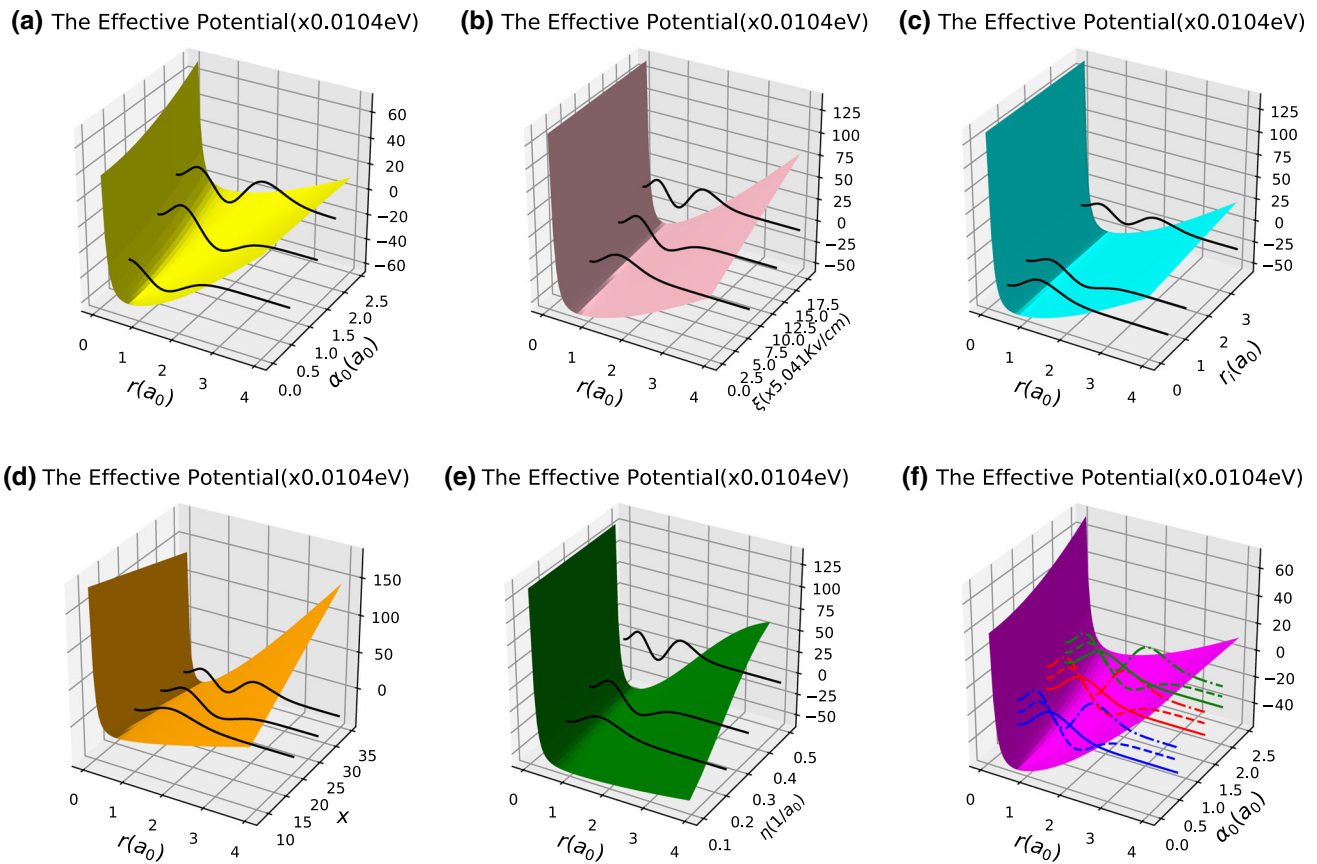
Fig. 1 The effective potential profile of the MQD as function of the radial distance $r(a_0)$ and, **a** the laser-dressed parameter ($\alpha_0(a_0)$), when $x = 0.4$, $\eta = 0.25/a_0$, $\xi = 5\text{kV/cm}$, $r_i = 0$ **b** the external electric field strength (ξ), when $x = 0.4$, $\eta = 0.25/a_0$, $\alpha_0 = 0.15a_0$, $r_i = 0$, **c** the impurity distance off the center ($r_i(a_0)$), when $x = 0.4$, $\eta = 0.25/a_0$, $\alpha_0 = 0.5a_0$, $\xi = 5\text{kV/cm}$, **d** *In*-concentration, when $\eta = 0.25/a_0$, $\alpha_0 = 0.15a_0$, $r_i = 0$, $\xi = 5$ kV/cm, **e** the dot's width parameter ($\eta(1/a_0)$), when $x = 0.4$, $\alpha_0 = 0.15a_0$, $r_i = 0$, $\xi = 5$ kV/cm, **f** same of (**a**) but three bound state wave functions for three different α_0-values. *Note* The effective potential profiles are for $\ell = 1$, and embedded wave functions are, respectively, the first, second excited and third excited states

(x) in Fig. 1d, the MQD width (η) in Fig. 1e, as a function of the radial distance (r). In Fig. 1f, the effective potential profile for three different values of the laser-dressing parameter (α_0) and the wave functions of the relevant localizations are represented.

In Fig. 2a, c, the effects of the incident optical intensity ($I(\text{W/m}^2)$) on the TRICs and TACs of the MQD including an impurity atom at its center are furnished, while the response of the carrier density ($\sigma_v(\text{m}^{-3})$) on the TRICs and TACs is shown in Fig. 2b, d. As seen in Fig. 2a, c, as the optical intensity increases, the resonant amplitudes of TRICs and TACs decrease, which arises from the increment in the nonlinear contribution. The optical intensity increment in TRICs and TACs amplitudes causes structural distortions in the MQD. The structural distortions are reflected in the TRICs and TACs amplitudes as instability. The TACs amplitudes have an unstable character at more feeble intensities compared to the TRICs ones (See $I = 0.2 \times 10^{10}\text{W/m}^2$ value in Fig. 2c). These results arising from the structural deterioration observed in the TACs properties due to the increasing intensity value, are crucial in determining the limit I for the TACs, especially in experimental studies. Here it should be also noted that the limit I-value depends on other parameter's values of the effective potential. In Fig. 2b, d, it is seen that the TRICs and TACs amplitudes increase as the electron density increases, which is an expected case.

In Fig. 3a, b, the TRICs and TACs of the MQD including centrally impurity atom are presented for different four values ($\alpha_0 = 0.1, 0.5a_0, 1a_0$ and $2a_0$) of the laser-dressing parameter as a function of the incident photon energy. The resonant amplitudes and frequencies of the TRICs and TACs are highly sensitive to the laser-dressing parameter. As the laser-dressing parameter increases, the TRICs and TACs resonant frequencies exhibit the red-shifting. Because, as can be seen in Fig. 1a, due to the increment of α_0, the effective potential width also increases as well as its repulsion. Since the dominant effect is the increase in potential width, the electrons have shallower localizations. As presented in the inset in Fig. 3a, b, the energy difference ΔE decreases with increasing α_0, which in turn confirm mentioned results. The fact that the energy differences can be tuned through the laser-dressing parameter makes the MQD an appropriate material for infrared detectors. The TRICs amplitudes increase with increasing α_0, which case is in line with expectations because the matrix elements ($|M|^+ = |M_{if}|^2$) increase due to increasing α_0 (See Fig. 3a inset). From the relevant observations, it is clear that the absorption amplitudes of $\alpha^{(1)}(\omega)$ and $\alpha^{(3)}(\omega)$ increase with increasing laser field strength. In Fig. 3b, the linear ($\alpha^{(1)}(\omega)$), nonlinear ($\alpha^{(3)}(\omega)$), and TACs ($\alpha(\omega)$) in the In_xGa_{1-x}As/GaAs MQD are presented as a function
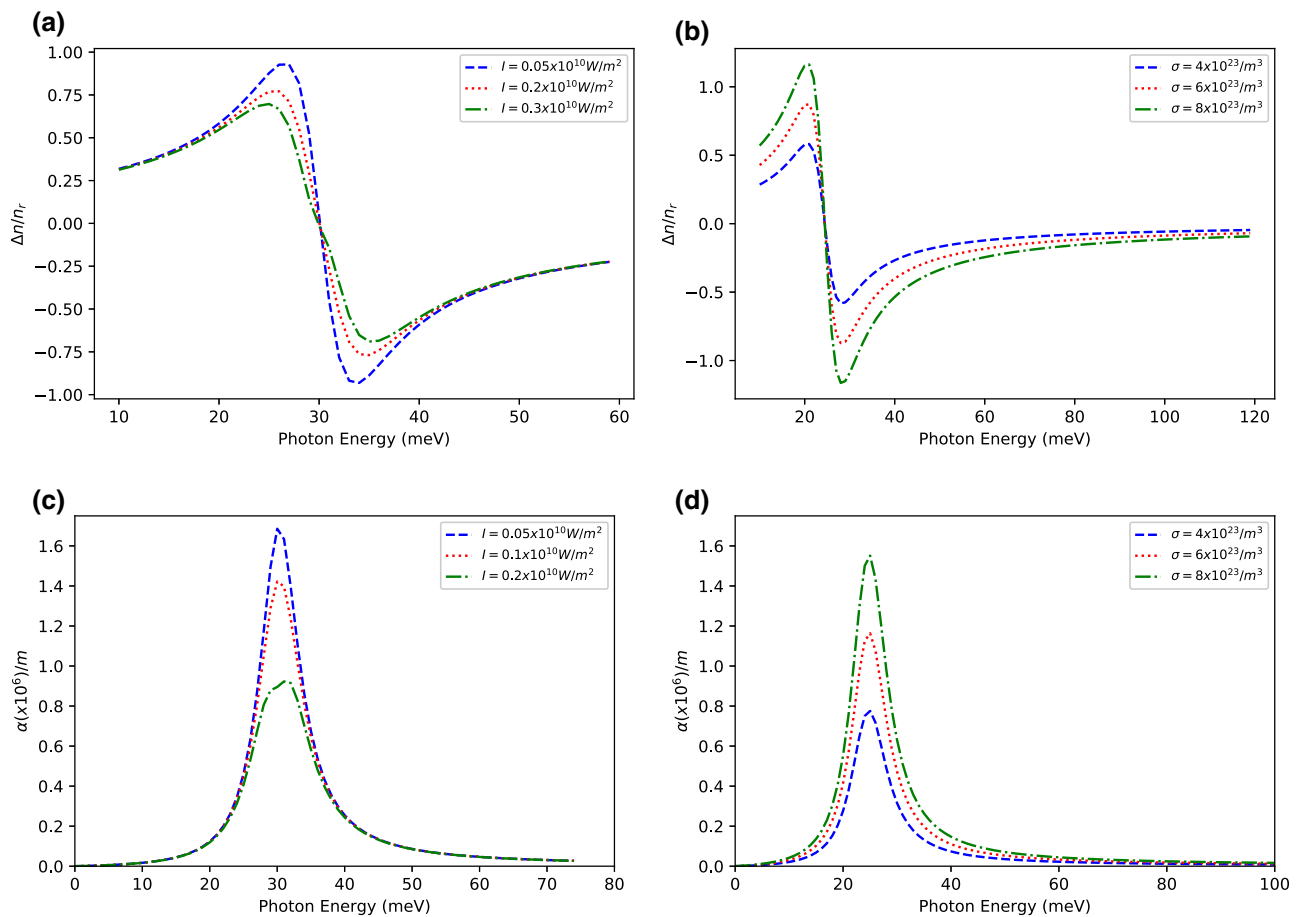
Fig. 2 a The TRICs versus I-changes, **b** the TRICs versus σ-changes, (c)the TACs versus I-changes, **d** the TACs versus σ-changes, of the MQD in consideration of $x = 0.4$, $\alpha_0 = 0.25a_0$, $\eta = 0.25/a_0$, $\xi = 5$ kV/cm, $r_i = 0$. When considering I, it is taken as $\sigma = 6 \times 10^{23}/m^3$, when examining σ it is taken as $I = 0.1 \times 10^{10}$ W/m^2
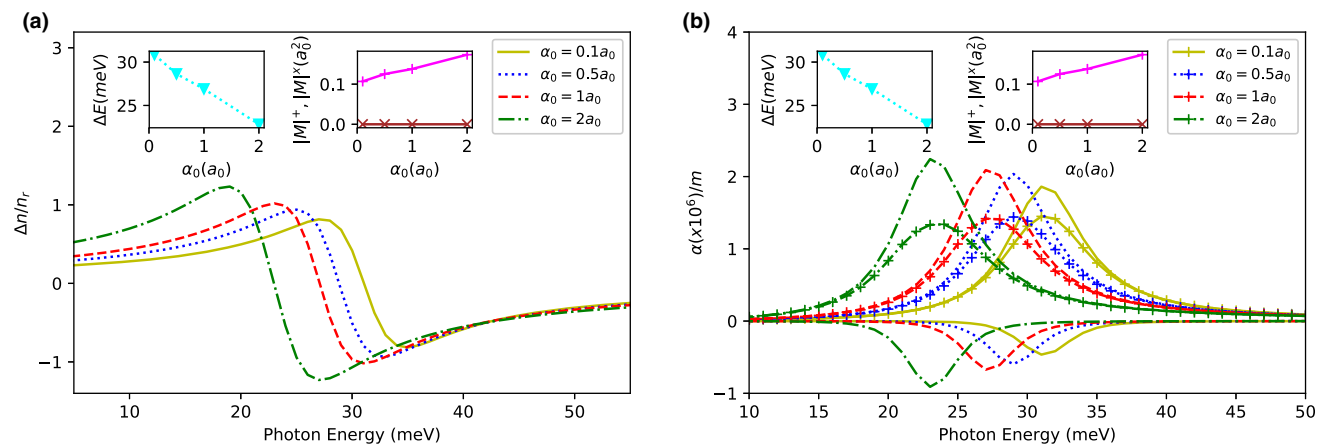

Fig. 3 a The TRICs and **b** TACs of the MQD with $x = 0.4$, $\eta = 0.25/a_0$, $r_i = 0$ for $\alpha_0 = 0.1 - 0.5 - 1 - 2a_0$ when $F = 5$kV/cm. The insets show the relevant energy differences and matrix elements, respectively, as $\Delta E = E_f - E_i$, $|M|^+ = |M_{if}|^2$, $|M|^x = |M_{ii} - M_{ff}|^2$, respectively. Plots with + in the TACs-plotting show the total absorption coefficients, while the others show linear and nonlinear contributions

of incident photon energy. It is observed in Fig. 3b that the TACs amplitudes obtained from the sum of the linear and nonlinear absorption coefficients exhibit a monotonous response to the change in laser field strength. Also, when considering the TRICs and TACs amplitudes, it is evident that the effect of $|M|^+$ on the amplitudes is more dominant compared to that of $|M|^x$.

In Fig. 4a, b, the TRICs and TACs of the MQD containing an impurity atom in its center are demonstrated for the external electric field values as $\xi = 0$, $\xi = 10$, $\xi = 30$ and $\xi = 90$ kV/cm, as a function of the incident photon energies. When investigating
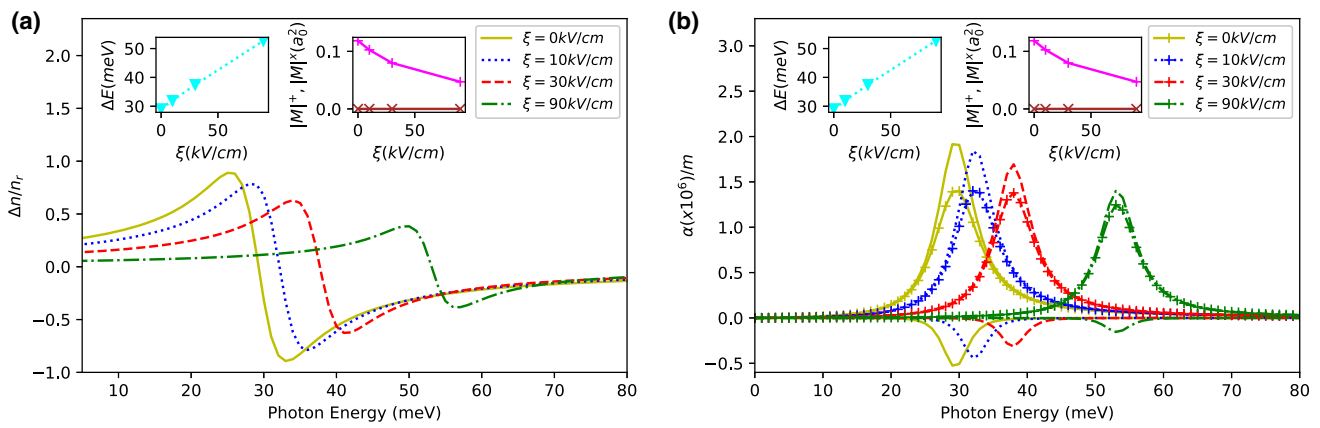
Fig. 4 a The TRICs and **b** TACs of the MQD with $x = 0.4$, $\eta = 0.25/a_0$, $r_i = 0$ for $\xi = 0 - 10 - 30 - 90 \text{kV/cm}$ when $\alpha_0 = 0.15a_0$. The insets show the relevant energy differences and matrix elements, respectively, as $\Delta E = E_f - E_i$, $|M|^+ = |M_{if}|^2$, $|M|^x = |M_{ii} - M_{ff}|^2$, respectively. Note: Plots with + in the TACs-plotting show the total absorption coefficients, while the others show linear and nonlinear contributions

these two graphs, a distinct blueshift is observed in the resonant frequencies of both TRICs and TACs because of increasing ξ. Because, the repulsion of the effective potential increases as the electric field increases, as can be clearly seen in Fig. 1b. Then, as the energy difference (ΔE) between the bound states increases with augmenting electric field, a significant blueshift occurs in the resonant frequencies of TRICs and TACs. The increment of the energy difference as a result of the increasing electric field is determined evidently in Fig. 4a, b insets. The TRICs amplitudes appear to be highly sensitive to the external electric field (Fig. 4a). The TRICs amplitudes also decrease markedly as a result of the increased electric field strength. As can be clearly seen in Fig. 4a inset, as the external electric field applied on the structure increases, the matrix elements decrease, which in turn causes to a dramatic decrement in the TRICs amplitudes as a result of increased electric field strength. In Fig. 4b, the TACs and its linear and nonlinear contributions are presented. The amplitudes of linear and nonlinear ACs decrease significantly depending on augmenting electric field strength, similar to the response of TRICs amplitudes to the electric field. However, TACs amplitudes decrease monotonically within linear-nonlinear dominance depending on the increasing electric field. Fig. 4b inset that presents the variation of the matrix elements to the electric field confirms this result.

In Fig. 5a, b, the TRICs and TACs of the MQD with a centrally impurity atom are given for the location values of the impurity atom ($r_i = 0.15a_0$, $0.75a_0$, $1.5a_0$, $3a_0$) as a function of the incident photon energies. As the impurity atom moves away from the center of the MQD up to $r_i = 1.5a_0$, the redshifting in the resonant frequencies of TRICs and TACs occurs. However, at positions after the impurity position $r_i = 1.5a_0$, the blue-shifting in the TRICs and TACs resonant frequencies constitutes. These observations are also confirmed by considering the variation with the impurity position of the energy difference (ΔE) between the bound states given in Fig. 5a, b insets. As can be clearly seen from these insets, while ΔE decreases with increasing position as the impurity atom moves away from the center up to $r_i = 1.5a_0$, ΔE starts to increase with the increasing impurity position after the $r_i = 1.5a_0$ value. This change arising from the position change in the energy differences causes the resonant frequencies of TRICs and TACs to shift first to red and then to blue. In Fig. 5a, it is seen that TRICs amplitudes increase for increments from $r_i = 0$ to $r_i = 1.5a_0$ and then decrease as the impurity closes from the center towards the quantum dot boundary. As can be clearly seen in Fig. 5a inset, the matrix elements ($|M^+|$, dominant) increase up to the $r_i = 1.5a_0$ value of the impurity position, while it starts to decrease after $r_i = 1.5a_0$ of the impurity position. This change in matrix elements causes to increment in the TRICs amplitudes up to $r_i = 1.5a_0$ and then decrement with increasing impurity position. In response to the impurity position variation, a remarkable agreement between the TRICs amplitudes and matrix elements is observed, as expected. In Fig. 5b, the amplitudes of linear and nonlinear ACs increase up to $r_i = 1.5a_0$ depending on the decentralization of the impurity location, similar to the variation of the TRICs amplitudes with position. However, it is evident that both the linear and nonlinear contribution amplitudes decrease in the augments after the $r_i = 1.5a_0$ value. It is clear that TACs amplitudes are monotonous despite considerably changes in the linear and nonlinear ones. Fig. 5b inset that shows the variation of matrix elements with impurity position confirms these observations. Because while the matrix elements increase with increasing position up to a certain value of the impurity position, after it starts to decrease.

In Fig. 6a, b, the TRICs and TACs of the MQD are given for $x = 0.15$, $x = 0.25$, $x = 0.35$ and $x = 0.45$ values of *In*-concentration, as a function of the incident photon energy. The increase in *In*-concentration (x) increases the effective potential strength and decreases its width, as seen in Fig. 1d. The increment in the effective potential strength leads to a blue-shift in the resonant frequencies of the TRICs and TACs. Because the increment in potential depth, that is, the increment in x, increases the energy difference (ΔE) (see Fig. 6a inset), a blue-shifting is observed in the TRICs and TACs resonant frequencies. The TRICs amplitudes decrease significantly as x increases, due to reducement in the matrix elements as a result of increasing x. In Fig. 6b, the change of the linear and nonlinear ACs and TACs amplitudes depending on the augment of x is seen. The linear and nonlinear ACs amplitudes decrease blatantly with increasing x, similar to the change of the TRICs amplitudes with concentration. However, the
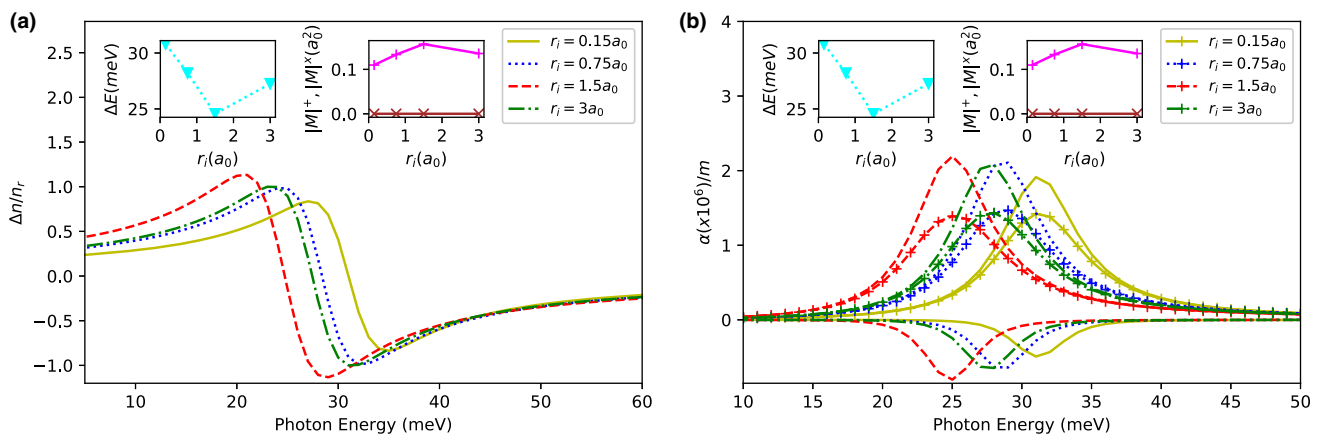
Fig. 5 **a** The TRICs and **b** the TACs of MQD with $x = 0.4$, $\eta = 0.25/a_0$, $r_i = 0.15 - 0.75 - 1.5 - 3a_0$ when $\alpha_0 = 0.25a_0$ and $\xi = 5$kV/cm. The insets show the relevant energy differences and matrix elements, respectively, as $\Delta E = E_f - E_i$, $|M|^+ = |M_{if}|^2$, $|M|^x = |M_{ii} - M_{ff}|^2$, respectively. *Note* Plots with + in the TACs-plotting show the total absorption coefficients, while the others show linear and nonlinear contributions
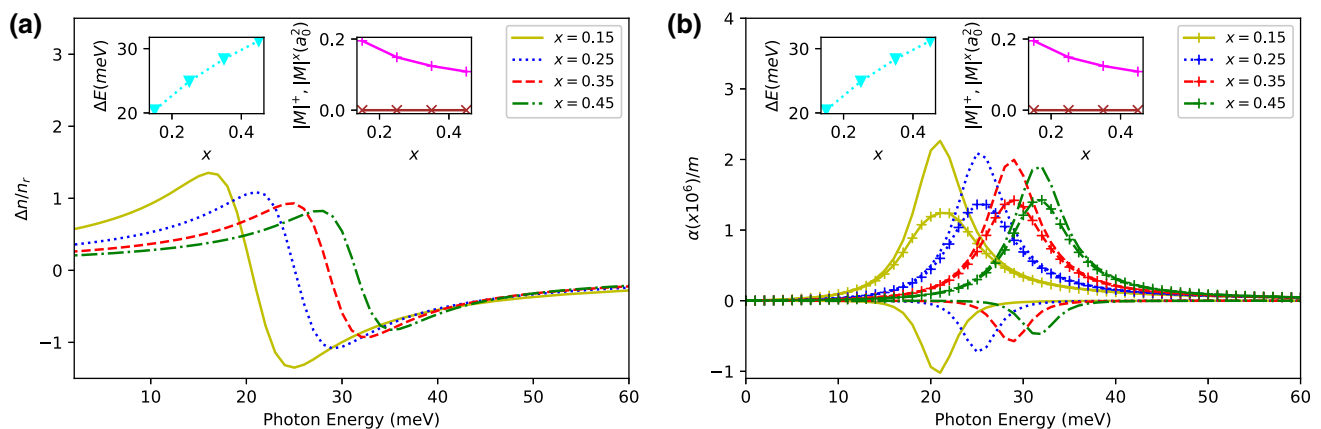

Fig. 6 **a** The TRICs and **b** the TACs of MQD with $x = 0.15 - 0.25 - 0.35 - 0.45$, $\eta = 0.25/a_0$, $r_i = 0$ when $\alpha_0 = 0.25a_0$ and $\xi = 5$kV/cm. The insets show the relevant energy differences and matrix elements, respectively, as $\Delta E = E_f - E_i$, $|M|^+ = |M_{if}|^2$, $|M|^x = |M_{ii} - M_{ff}|^2$, respectively. *Note* Plots with + in the TACs-plotting show the total absorption coefficients, while the others show linear and nonlinear contributions

TACs amplitudes increase monotonically. The reason for this case is that the linear and nonlinear contribution decrease at different rates compared to each other.

In Fig. 7a, b, the TRICs and TACs of the MQD are furnished for $\eta = 0.25/a_0$, $\eta = 0.35/a_0$, $\eta = 0.45/a_0$ and $\eta = 0.50/a_0$ values of the quantum dot width parameter as a function of the incident photon energy. Since the enhancement of η strengthens the encompassment effect (see Fig. 1e), the energy difference in Fig. 7a, b insets increases due to increasing η. Therefore, a blatant blueshift occurs in the TRICs and TACs resonant frequencies. The TRICs amplitudes decrease dramatically due to increasing η, which is due to the decrease in matrix elements by increasing η, as seen in Fig. 7a inset. The shifts in TRICs resulting from η are also valid for the linear and nonlinear ACs amplitudes presented in Fig. 7b. But, the change of TACs amplitudes with η is monotonous because there is a combined effect of the linear and nonlinear contributions of absorption coefficients.

4 Conclusion

The optical properties of the $In_xGa_{1-x}As$/GaAs MQD containing different positioned impurity atom under the laser and electric field have been probed. The results can be outlined as: Under the considered physical conditions, the TRICs character of MQD is more stable compared to that of the TACs character. Because, the TRICs display no distortion at $I = 0.3 \times 10^{10}$ W/m^2, while the TACs $I = 0.2 \times 10^{10}$ W/m^2 tends to become unstable. The laser field is an important external factor for both the resonant frequencies and the optimization of the quantum dot, because it produces observable effects. The external electric field is also an important external factor, and may be said to be more functional in terms of resonant frequencies and amplitudes compared to the laser field. The position of the impurity atom leads to remarkable outcomes. The value $r_i = 1.5a_0$ turns into reversible the optical property of the structure. In this context, under the considered conditions, this $r_i = 1.5a_0$ value for the structure becomes a special
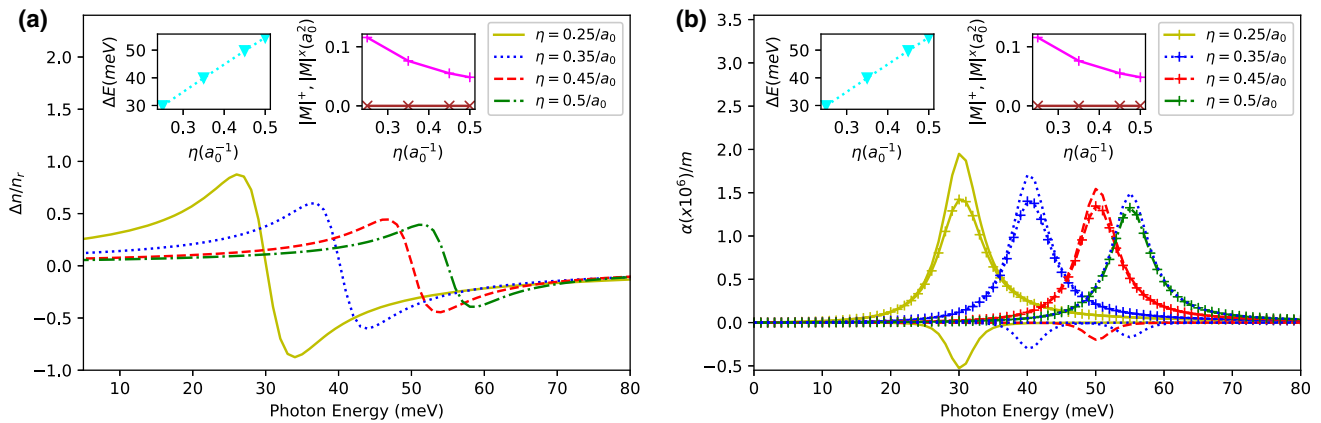
Fig. 7 **a** The TRICs and **b** the TACs of MQD with $x = 0.4$, $\eta = 0.25 - 0.35 - 0.45 - 0.5 a_0^{-1}$, $r_i = 0$ when $\alpha_0 = 0.25 a_0$ and $\xi = 5$kV/cm. The insets show the relevant energy differences and matrix elements, respectively, as $\Delta E = E_f - E_i$, $|M|^+ = |M_{if}|^2$, $|M|^x = |M_{ii} - M_{ff}|^2$, respectively. *Note* Plots with + in the TACs-plotting show the total absorption coefficients, while the others show linear and nonlinear contributions

value. However, it is important to say that this special value may change if other parameter values change. As expected, structural parameters are more effective compared to the external field parameters. However, considering the practicality of external field effects, the determination of the results they cause and the fixing of their functional ranges are substantial in terms of experimental research. If the external field effects can be an alternative to the structural effects in consideration of the electronic and optical specifications, some advantages can be achieved in the application area. In this manner, optically, the laser field is an alternative to the effect of relocation of the impurity atom up to $r_i = 1.5 a_0$. The increment in external electric field is an alternative to the increase in the *In*-concentration and the increase in the quantum dot width parameter (η). The impurity position change for increments after $r_i = 1.5 a_0$ can also include in this alternativeness.

Data availability statement The data generated during the current study are accessible. [Authors' comment: The data would be available on reasonable request.]

Declarations

Conflict of interest The authors report no conflict of interest.

References

1. A. Tartakovskii, *Quantum Dots Optics, Electron Transport and Future Applications* (Cambridge University Press, Cambridge, 2012)
2. A.D. Yoffe, Semiconductor quantum dots and related systems: electronic, optical, luminescence and related properties of low dimensional systems. Adv. Phys. **50**(1), 1 (2001)
3. M. Nirmal, L. Brus, Luminescence photophysics in semiconductor nanocrystals. Acc. Chem. Res. **32**, 407 (1999)
4. E.H. Sargent, Colloidal quantum dot solar cells. Nat. Photon. **6**(3), 133 (2012)
5. I. Lagraa, B. Soudini, H. Abid, S. Taleb, Study and optimization of structure InAs/InGaAs quantum dot in-a-well long-wave infrared photodetector. Optik **251**, 168494 (2022)
6. A.J. Shields, M.P. O'Sullivan, I. Farrer, D.A. Ritchie, M.L. Leadbeater, N.K. Patel, R.A. Hogg, C.E. Norman, N.J. Curson, M. Pepper, Single photon detection with a quantum dot transistor. Jpn. J. Appl. Phys. **40**, 2058–2064 (2021)
7. V. Aroutiounian, S. Petrosyan, A. Khachatryan, Quantum dot solar cells. J. Appl. Phys. **89**, 2268 (2001)
8. D.E. Fouskidis, K.E. Zoiros, A. Hatziefremidis, Reconfigurable all-optical logic gates (AND, NOR, NOT, OR) with quantum-dot semiconductor optical amplifier and optical filter. IEEE J. Sel. Top. Quantum Electron. **27**, 7600915 (2021)
9. S. Ma, Z. Chen, H. Sun, N.K. Dutta, High speed all optical logic gates based on quantum dot semiconductor optical amplifiers. Opt. Express **8**, 6417 (2010)
10. P. Baser, M.K. Bahar, Evaluation of the external electric- and magnetic field-driven Mathieu quantum dot's optical observables. Physica B **639**, 413991 (2022)
11. J.N.L. Connor, T. Uzer, R.A. Marcus, Eigenvalues of the Schrödinger equation for a periodic potential with nonperiodic boundary conditions: A uniform semiclassical analysis. J. Chem. Phys. **80**, 5095 (1984)
12. H. Panahı, M. Baradaran, S.R. Azızıan, Solutıons of the quası-exactly solvable mathıeu potentıal by the asymptotıc iteratıon method. Romanian Rep. Phys. **68**, 56 (2016)
13. D.S. Jiang, Y.H. Zhang, C. Abraham, K. Syassen, J.B. Xia, K. Ploog, A study of resonant Raman scattering in GaInAs/AlInAs multiple quantum wells. Superlattices Microstruct. **12**, 273 (1992)

14. Y. He, W. Yan, Fabrication and simulation of GaInAs Solar cells using compositionally step-graded AlGaInAs buffers on GaAs substrate. Opt. Quant. Electron. **52**, 372 (2020)
15. W. Gillin, Y.S. Tang, N.J. Whitehead, K.P. Homewood, B.J. Sealy, M.T. Emeny, C.R. Whitehouse, Thermal processing of strained GaInAs/GaAs high hole mobility transistor structures. Appl. Phys. Lett. **56**, 1116 (1990)
16. D. Schlenker, T. Miyamoto, Z. Chen, F. Koyama, Member, IEEE, and K. Iga 1.17- m Highly Strained GaInAs-GaAs Quantum-Well Laser, IEEE Photonics Technology Letters, 11, 946, (1999)
17. C. Thirstrup, Novel electro-optical phase modulator based on GaInAs/InP modulation-doped quantum-well structures. Appl. Phys. Lett. **61**, 2641 (1992)
18. H. Deng, Q. Yang, Z. Wang, X. Guo, H. Shao, X. Li, H. Gong, InGaAs short wavelength infrared detector based on carrier collection effect. Infrared Device and Infrared Technology **12061**, 407 (2021)
19. G. Rezaei, B. Vaseghi, J. Ebrahimi, External electric field effects on the electronic and hydrogenic impurity states in ellipsoidal and semi-ellipsoidal quantum dots. Superlattices Microstruct. **49**, 591 (2011)
20. F. Ungan, M.K. Bahar, Optical specifications of laser-induced Rosen–Morse quantum well. Opt. Mater. **90**, 231 (2019)
21. S. Aktas, A. Bilekkaya, F.K. Boz, S.E. Okan, Electron transmission in symmetric and symmetric double-barrier structures controlled by laser fields. Superlattices Microstruct. **85**, 266 (2015)
22. R.Y. Yan, J. Tang, Z.H. Zhang, Optical properties in GaAs/AlGaAs semiparabolic quantum wells by the finite difference method: combined effects of electric field and magnetic field. Int. J. Mod. Phys. B **32**, 1850159 (2018)
23. E.C. Niculescua, L.M. Burileanu, Nonlinear optical absorption in inverse V-shaped quantum wells modulated by high-frequency laser field. Eur. Phys. J. B **74**, 117 (2010)
24. M.J. Karimi, H. Vafaei, Second-order nonlinear optical properties in a strained InGaN/AlGaN quantum well under the intense laser field. Superlattices Microstruct. **78**, 1 (2015)
25. D. Brunne, M. Lafrentz, V.V. Pavlov, R.V. Pisarev, A.V. Rodina, D.R. Yakovlev, M. Bayer, Electric field effect on optical harmonic generation at the exciton resonances in GaAs. Phys. Rev. B **92**, 085202 (2015)
26. A.D. Yoffe, Semiconductor quantum dots and related systems: electronic, optical, luminescence and related properties of low dimensional systems. Adv. Phys. **50**, 1 (2001)
27. C. Xia, Z. Zeng, S. Wei, Electron and impurity states in GaN/AlGaN coupled quantum dots: effects of electric field and hydrostatic pressure. J. Appl. Phys. **108**, 054307 (2010)
28. Gh. Safarpour, M.A. Izadi, E. Niknam, M. Moradi, M.M. Golshan, Simultaneous effects of external electric field and aluminum concentration on the binding energy of a laser-dressed donor impurity in a spherical quantum dot confined at the center of a cylindrical nano-wire. Phys. B **436**, 14 (2014)
29. W. Xie, Y. Chen, Optical absorption and refractive index of a donor impurity in a three-dimensional quantum pseudodot. Superlattices Microstruct. **50**, 691 (2011)
30. E.C. Niculescu, D. Bejan, Off-centre impurity-related nonlinear optical absorption, second and third harmonic generation in a two-dimensional quantum ring under magnetic field. Philos. Mag. **97**(24), 2089–2107 (2017)
31. S. Saha, S. Pal, J. Ganguly, M. Ghosh, Exploring optical refractive index change of impurity doped quantum dots driven by white noise. Superlattices Microstruct. **88**, 620 (2015)
32. A. Mandal, S. Sarkar, A.P. Ghosh, M. Ghosh, Analyzing total optical absorption coefficient of impurity doped quantum dots in presence of noise with special emphasis on electric field, magnetic field and confinement potential. Chem. Phys. **463**, 149 (2015)
33. J. Ganguly, S. Saha, S. Pal, M. Ghosh, Noise-driven optical absorption coefficients of impurity doped quantum dots. Physica E **75**, 246 (2016)
34. J. D. Jackson, Classical Electrodynamics, Third Edition, Wiley, 1999
35. B.H. Bransden, C.J. Joachain, *Physics of Atoms and Molecules* (Prentice-Hall, Upper Saddle River, 2003)
36. W.C. Henneberger, Perturbation method for atoms in intense light beams. Phys. Rev. Lett. **21**, 838 (1968)
37. H.A. Kramers, *Collected Scientific Paper*, vol. 866 (North-Holland, Amsterdam, 1956)
38. F.M.S. Lima, M.A. Amato, L.S.F. Olavo, O.A.C. Nunes, A.L.A. Fonseca, E.F. da Silva, Jr., Intense laser field effects on the binding energy of impurities in semiconductors. Phys. Rev. B **75**, 073201 (2007)
39. M. Gavrila, J.Z. Kaminski, Free-free transitions in intense high-frequency laser fields. Phys. Rev. Lett. **52**, 613 (1984)
40. F. Ehlotzky, Scattering phenomena in strong radiation fields II. Can. J. Phys. **63**, 907 (1985)
41. F. Ehlotzky, Positronium decay in intense high frequency laser fields. Phys. Lett. A **126**, 524 (1988)
42. M.K. Bahar, Effects of laser radiation field on energies of hydrogen atom in plasmas. Phys. Plasmas **22**, 092709 (2015)
43. M.K. Bahar, A. Soylu, Laser-driven two-electron quantum dot in plasmas. Phys. Plasmas **25**, 062113 (2018)
44. M.K. Bahar, A. Soylu, Two-electron pseudodot system with laser effect in plasmas. IEEE Trans. Plasma Sci. **47**, 1713 (2019)
45. M. Kalinski, J.H. Eberly, New states of hydrogen in a circularly polarized electromagnetic field. Phys. Rev. Lett. **77**, 2420 (1996)
46. B.N. Datta, *Numerical Linear Algebra and Applications*, 2nd edn. (SIAM, Philadelphia, 2010)
47. R.W. Boyd, *Nonlinear Optics*, 3rd edn. (Rochester, New York, 2007)
48. K. Kılıç, M.K. Bahar, Optical response of plasma processed quantum dot under the external fields. Int. J. Quantum Chem. **121**, e26564 (2021)
49. S. Paul, J.B. Roy, P.K. Basu, Empirical expressions for the alloy composition and temperature dependence of the band gap and intrinsic carrier density in $Ga_x In_{1-x}As$. J. Appl. Phys. **69**, 827 (1991)
50. F. Ungan, M.K. Bahar, M.G. Barseghyan, L.M. Perez, D. Laroze, Effect of intense laser and electric fields on nonlinear optical properties of cylindrical quantum dot with Morse potential. Optik **236**, 16662 (2021)